






Article

Synthesis and Characterization of Dendronized Gold Nanoparticles Bearing Charged Peripheral Groups with Antimicrobial Potential

Gabriel Perli ¹, Diego L. Bertuzzi ¹, Dênio E. P. Souto ^{1,2}, Miguel D. Ramos ¹, Carolyne B. Braga ¹, Samile B. Aguiar ¹ and Catia Ornelas ^{1,*}

¹ Institute of Chemistry, University of Campinas, Campinas 13083-970, Brazil; perligabriel@gmail.com (G.P.); diego.bertuzzi@hotmail.com (D.L.B.); denio.souto@ufpr.br (D.E.P.S.); migueljr.qma@gmail.com (M.D.R.); carolbbraga7@gmail.com (C.B.B.); samilede17@gmail.com (S.B.A.)

² Laboratorio de Espectrometria, Sensores e Biosensores, Departamento de Quimica, Universidade Federal do Paraná (UFPR), Curitiba 81531-980, Brazil

* Correspondence: catiaornelas@catiaornelaslab.com

Abstract: Dendronized gold nanoparticles (AuNPs) were synthesized bearing charged peripheral groups. Two novel AB₃-type dendrons were synthesized with a thiol group at the focal point followed by their attachment to AuNPs. Dendrons were designed to have nine charged peripheral groups (carboxyl or amine), glycol solubilizing, units and one thiol moiety at the focal point. Both dendrons and all intermediates were synthesized in high yields and characterized by nuclear magnetic resonance spectroscopy (NMR) and mass spectrometry (MS). The amine- and carboxyl-terminated dendrons were used to functionalize gold nanoparticles (AuNPs) previously stabilized with citrate. The nanoparticles' diameters and their colloidal stability were investigated using dynamic light scattering (DLS). The size and morphology of the dendronized AuNPs were evaluated by scanning electron microscopy (SEM), which revealed individual particles with no aggregation after replacement of citrate by the dendrons, in agreement with the DLS data. The absorption spectroscopy reveals a prominent plasmonic band at 560 nm for all AuNPs. The zeta potential further confirmed the expected charged structures of the dendronized AuNPs. Considering all the physical–chemical properties of the charged dendronized AuNPs developed in this work, these AuNPs might be used as a weapon against multi-drug resistant bacterial infections.

Keywords: macromolecules; dendrons; gold nanoparticles; dendronized nanoparticles; antimicrobial; drug delivery



Citation: Perli, G.; Bertuzzi, D.L.; Souto, D.E.P.; Ramos, M.D.; Braga, C.B.; Aguiar, S.B.; Ornelas, C. Synthesis and Characterization of Dendronized Gold Nanoparticles Bearing Charged Peripheral Groups with Antimicrobial Potential. *Nanomaterials* **2022**, *12*, 2610. <https://doi.org/10.3390/nano12152610>

Academic Editors: Shiao-Wen Tsai and Hsi-Chin Wu

Received: 14 June 2022

Accepted: 25 July 2022

Published: 29 July 2022

Publisher's Note: MDPI stays neutral with regard to jurisdictional claims in published maps and institutional affiliations.



Copyright: © 2022 by the authors. Licensee MDPI, Basel, Switzerland. This article is an open access article distributed under the terms and conditions of the Creative Commons Attribution (CC BY) license (<https://creativecommons.org/licenses/by/4.0/>).

1. Introduction

The evolution of multi-drug resistant (MDR) microorganisms has become a severe threat to public health worldwide. According to the last predictions, infections caused by antimicrobial-resistant germs will result in 10 million annual deaths by 2050, exceeding cancer-related mortality [1–3]. Due to the risk of these infections and the lack of innovation in this area over the last fifteen years, the quest for new antimicrobial strategies has played a crucial role in science [1,4–6]. Nanoparticles (NPs) have been proposed as great candidates for such therapeutic applications owing to their unique characteristics. NPs have a high surface-to-volume ratio that enables enhanced contact with the target organisms [7–11]. NPs can also interact with bacterial cells to regulate the uptake and molecular pathways [12–14]. In particular, gold nanoparticles (AuNPs) exhibit additional attributes to help in this endeavor, including chemical stability, biocompatibility, commercial availability, easy functionalization, and high intrinsic antimicrobial activity [15–19]. AuNPs also possess remarkable optical properties related to plasmon absorption, which allow their use in photothermal-induced antibacterial therapy [20,21].

Several reports show enhanced activity of AuNPs bearing antibacterial agents, making clear that the combination of classical antibiotics and AuNPs is a powerful strategy to overcome antibiotic resistance [22,23]. Payne et al. reported that AuNPs grafted with kanamycin have significant antibacterial activity against Gram-positive *Staphylococcus epidermis* and the Gram-negative *Enterobacter aerogenes* [24]. Rattanata et al. observed enhanced bactericidal activity of gallic acid with AuNPs, and demonstrated that AuNPs were able to deliver gallic acid through the bacterial cell membrane and interact with DNA [25].

The intrinsic antimicrobial activity of AuNPs has been shown to be dependent on the nanoparticles' size, surface chemistry, and type of ligands [8,9,16,26–30]. In this context, the use of dendrimers or dendrons to coat AuNPs is an interesting approach due to the combination of desirable properties from both nanomaterials, since dendrimers and dendrons also exhibit intrinsic antimicrobial activity that is dependent on the dendrons' functionalization [31–33].

Dendrimers and dendrons are a special class of macromolecules with monodispersed architectures and a high density of terminal functional groups [34–36]. These molecules are synthesized in a stepwise fashion resulting in well-defined structures [34,35]. The controlled synthetic strategies used to build dendrimers and dendrons allow precise control over the nanoscale size, shape, number, nature, and location of functional groups [37,38].

Dendrimers are commonly radially symmetric macromolecules, whereas dendrons have AB_x branched structures: where B represents the terminal functional groups and A represents one reactive group at the focal point [34,35,39]. The functional group at the focal point can be used as an anchor for stabilizing metal NPs [40,41], and the active termini may be used to attach a high density of charged groups per macromolecule [42–44]. Indeed, their high performance in biomedical applications arise from multivalent interactions and secondary interactions between the dendrimer termini with biomolecules on the target human cells or bacteria [42,45–48].

For instance, classical antibiotics, charged groups, targeting groups, and/or solubilizing units may be attached to a single dendrimer, allowing the construction of novel smart carriers with tunable properties [49–51]. Although the use of branched molecules as nanocarriers is a well-investigated area, there is room for developing dendron-based antimicrobials [42].

Herein, we report the synthesis of two novel well-defined dendrons designed to have amide and glycol solubilizing units in the backbone, one thiol group at the focal point, and nine carboxyl or amine termini. The ethylene glycol derivatives were used to improve water solubility and biocompatibility. The thiol group at the focal point ensures the anchoring on AuNPs, and the charged terminal groups were designed to enhance the antimicrobial effect by interacting with the outer membranes of bacteria.

To decrease the steric hindrance at the focal point of dendrons, a bi-functional glycol spacer was designed to have a protected thiol group and a free carboxylic acid. A second-generation Newkome-type dendron was synthesized and decorated with ethylene glycol derivatives. The resultant dendrons were then attached to the synthesized glycol spacer via amidation. The final dendrons with a free thiol group at the focal point were obtained after sequential deprotection reactions. The dendrons were attached to the surface of AuNPs through the ligand exchange strategy with AuNPs stabilized with citrate. The effect of the ligand replacement over the size, stability, charge, and electronic properties of the dendron-coated AuNPs was analyzed using dynamic light scattering (DLS), zeta potential, UV-vis spectroscopy, and scanning electron microscopy (SEM). We rationalized that the combination of the intrinsic antimicrobial properties of AuNPs and dendrimers allied to the positively or negatively charged surface of the new dendronized AuNPs may result in nanoparticles with enhanced antimicrobial activity.

2. Materials and Methods

2.1. Materials

All chemicals were purchased from Sigma–Aldrich (St. Louis, MO, USA) and used without further purification. Reactions dealing with air- and moisture-sensitive compounds were carried out using a Schlenk line. Solvents were freshly distilled using a proper drying agent for each case, except for dimethylformamide (DMF), which was purchased as an anhydrous grade in a sealed flask and used under nitrogen atmosphere.

2.2. Methods

2.2.1. Synthesis of Compound 2

In a Schlenk flask, tert-Butyl 12-hydroxy-4,7,10-trioxadodecanoate (0.90 mmol, 250.00 mg), N,N-diisopropylethylamine (1.4 eq, 1.26 mmol, 163.85 mg, 0.220 mL), and p-toluenesulfonyl chloride (1.3 eq, 1.17 mmol, 223.1 mg) were dissolved in 10 mL of anhydrous dichloromethane. The mixture was stirred under N₂ atmosphere for 12 h at room temperature. The solvent was removed using rotary evaporation and the crude product was purified by column chromatography using silica gel and dichloromethane:methanol (solvent mixture gradient from 100:0 until 95:5) as eluent. Compound 2 was obtained as a colorless oil in 98% of yield (381.1 mg). ¹H NMR (CDCl₃, 500 MHz), δ (ppm): 7.75 (d, *J* = 8.0 Hz, ArH, 2H), 7.30 (d, *J* = 8.0 Hz, ArH, 2H), 4.12 (t, *J* = 5 Hz, CH₂O, 2H), 3.66–3.52 (m, CH₂OCH₂CH₂OCH₂CH₂O, 10H), 2.45 (t, *J* = 6.5 Hz, CH₂CO, 2H), 2.39 (s, ArCH₃, 3H), 1.39 (s, COOC(CH₃)₃, 9H). ¹³C NMR (CDCl₃, 500 MHz), δ (ppm): 171.9 (COOtBu), 144.8 (ArC_q), 133.0 (ArC_q), 129.8 (ArCH), 127.9 (ArCH), 80.5 C(CH₃)₃, 70.7–66.9 (CH₂OCH₂CH₂OCH₂CH₂O), 36.3 (CH₂COOtBu), 28.1 C(CH₃)₃, 21.6 (ArCH₃). ESI-QTOF-MS [M+H]⁺ *m/z* calcd for C₂₀H₃₂O₈SH: 433.18, found: 433.23.

2.2.2. Synthesis of Compound 3

In a round-bottom flask, compound 2 (0.81 mmol, 381.1 mg) was dissolved in 1.5 mL of deionized water and 13.5 mL of formic acid. The mixture was stirred at room temperature for 12 h. The aqueous solution was evaporated to dryness using rotary evaporation, and the resulting solid was washed with diethyl ether (3 × 30 mL). Compound 3 was obtained as a white powder in quantitative yield (301.6 mg). ¹H NMR (CDCl₃, 500 MHz), δ (ppm): 7.80 (d, *J* = 8.0 Hz, ArH, 2H), 7.32 (d, *J* = 8.0 Hz, ArH, 2H), 4.16 (t, *J* = 5 Hz, CH₂O, 2H), 3.79–3.60 (m, CH₂OCH₂CH₂OCH₂CH₂O, 10H), 2.67 (t, *J* = 6.5 Hz, CH₂CO, 2H), 2.42 (s, ArCH₃, 3H). ¹³C NMR (CDCl₃, 500 MHz), δ (ppm): 176.2 (COOH), 145.1 (ArC_q), 131.5 (ArC_q), 130.0 (ArCH), 128.1 (ArCH), 80.5 C(CH₃)₃, 70.8–66.4 (CH₂OCH₂CH₂OCH₂CH₂O), 34.8 (CH₂COOH), 21.8 (ArCH₃). ESI-QTOF-MS [M+H]⁺ *m/z* calcd for C₁₆H₂₄O₈SH: 377.12, found: 377.21.

2.2.3. Synthesis of Compound 4

In an air-free Schlenk flask, compound 3 (0.80 mmol, 301.6 mg) and potassium thioacetate (1.5 eq, 1.2 mmol, 137.1 mg) were dissolved in 10 mL of anhydrous N,N-dimethylformamide. The mixture was stirred under N₂ atmosphere for 24 h at room temperature. The reaction mixture was washed with deionized water (3 × 10 mL), and the organic phase was dried over Na₂SO₄, filtered, and concentrated under vacuum. The crude product was further purified by column chromatography using silica gel and dichloromethane:methanol (solvent mixture gradient from 100:0 to 90:10) as eluent. Compound 4 was obtained as a yellowish oil in 85% of yield (190.5 mg). ¹H NMR (CDCl₃, 500 MHz), δ (ppm): 3.78–3.58 (m, CH₂OCH₂CH₂OCH₂CH₂O, 10H), 3.09 (t, *J* = 8.5 Hz, SCH₂O, 2H), 2.64 (t, *J* = 7.5 Hz, CH₂COOH), 2.33 (s, S(CO)CH₃, 3H). ¹³C NMR (CDCl₃, 500 MHz), δ (ppm): 195.9 (CH₃(CO)S), 176.2 (COOH), 70.7–66.5 (CH₂OCH₂CH₂OCH₂CH₂O), 34.9 (CH₂S(CO)CH₃), 30.7 (CH₂COOH), 29.0 (S(CO)CH₃). ESI-QTOF-MS [M+H]⁺ *m/z* calcd for C₁₁H₂₀O₆SH: 281.10, found: 281.11.

2.2.4. Synthesis of Compound 6

In an air-free Schlenk flask, compound 5 (0.51 mmol, 590 mg), *N,N*-diisopropylethylamine (1.4 eq, 0.71 mmol, 92.3 mg, 0.124 mL), and HATU (1.4 eq, 0.71 mmol, 0.271 g) were dissolved in 15 mL of anhydrous *N,N*-dimethylformamide. The mixture was stirred for 15 min under nitrogen atmosphere, and the *N*-Boc-2,2'-(ethylenedioxy)diethylamine (9.5 eq, 4.85 mmol, 1.2 g, 1.15 mL) was slowly added using a proper needle and syringe. The mixture was stirred for 48 h at room temperature and under nitrogen atmosphere. The organic solvent was removed by rotary evaporation, followed by washing with deionized water (10 × 20 mL). The product was further purified by column chromatography using silica gel and dichloromethane:methanol (solvent mixture gradient from 100:0 to 95:5) as eluent. Compound 6 was obtained as a yellowish oil with 85% of yield (1.4 g). ¹H NMR (CDCl₃, 600 MHz), δ (ppm): 7.74 (d, *J* = 8.7 Hz, ArH, 2H), 7.63 (d, *J* = 8.7 Hz, ArH, 2H), 7.37 (t, *J* = 8.4 Hz, ArH, 2H), 7.30 (t, *J* = 8.4 Hz, ArH, 2H), 7.08 (s, CONH, 9H), 6.19 (s, CONH, 1H), 5.35 (s, CH₂CONH, 9H), 4.26 (br d, CH₂CONH, 2H), 4.18 (br t, CHCH₂CONH, 1H), 3.56–3.51 (br t, CH₂OCH₂CH₂OCH₂, 72H), 3.50–3.48 (br t, CONHCH₂, 18H), 3.36–3.27 (br t, CH₂NHCOOtBu, 18H), 2.18 (br t, CH₂CO, 24H), 1.98 (br t, HCCH₂, 24H), 1.41 (s, (CO)OC(CH₃)₃, 81H). ¹³C NMR (CDCl₃, 600 MHz), δ (ppm): 173.6 (CH₂(CO)NH), 173.4 (CH₂(CO)NH), 156.3 (NH(CO)OtBu), 155.0 (NH(CO)OtBu), 144.7–120.1 (Fmoc-Ar 13C), 79.3 (C_q(CH₃)₃), 70.3–69.8 (CH₂OCH₂CH₂O), 66.2 (CCH₂O), 58.0 (OCH₂CH₂NH), 57.4 (NHC_q), 47.4 (CCH₂O), 41.7 (NHC_q), 40.4 (HNCH₂), 39.4 (CH₂NH), 31.6 (CH₂CONH), 30.9 (HNC_qCH₂), 29.8–28.6 (CH₂CH₂CO), 28.6 (OC(CH₃)₃). MALDI-TOF-MS [M+Na]⁺ *m/z* calcd for C₁₅₄H₂₇₀N₂₂O₅₀Na: 3251.35, found: 3251.70.

2.2.5. Synthesis of Compound 7

In an air-free Schlenk flask, compound 5 (0.51 mmol, 590 mg), *N,N*-diisopropylethylamine (1.4 eq, 0.71 mmol, 92.3 mg, 0.124 mL), and HATU (1.4 eq, 0.71 mmol, 0.271 g) were dissolved in 15 mL of anhydrous *N,N*-dimethylformamide. The mixture was stirred for 15 min under nitrogen atmosphere, and the tert-butyl 12-amino-4,7,10-trioxadodecanoate (9.5 eq, 4.85 mmol, 1.34 g, 1.20 mL) was slowly added using a proper needle and syringe. The mixture was stirred for 48 h at room temperature and under nitrogen atmosphere. The organic solvent was removed by rotary evaporation, followed by washing with deionized water (10 × 20 mL). The product was further purified by column chromatography using silica gel and dichloromethane:methanol (solvent mixture gradient from 100:0 to 94:6) as eluent. Compound 7 was obtained as a yellow oil with 95% of yield (1.69 g). ¹H NMR (CDCl₃, 600 MHz), δ (ppm): 8.4 (d, *J* = 8.7 Hz, ArH, 2H), 7.63 (br d, ArH, 2H), 7.35 (t, *J* = 8.4 Hz, ArH, 2H), 7.27 (t, *J* = 8.4 Hz, ArH, 2H), 4.47 (br d, CH₂CONH, 2H), 4.17 (br t, CHCH₂CONH, 1H), 3.68 (t, *J* = 7.8 Hz, OCH₂CH₂, 18H), 3.67–3.65 (m, OCH₂CH₂OCH₂CH₂O, 72H), 3.47 (br t, CH₂O, 18H), 3.33 (br t, NHCH₂, 18H), 2.48 (t, *J* = 7.8 Hz, CH₂(CO)OtBu, 18H), 2.47 (br t, CH₂CO, 24H), 2.18 (br t, HCCH₂, 24H), 1.41 (s, (CO)OC(CH₃)₃, 81H). ¹³C NMR (CDCl₃, 600 MHz), δ (ppm): 173.7 ((CO)OtBu), 171.2 (CH₂(CO)NH), 155.1 (NH(CO)C_q), 144.2–120.0 (Fmoc-Ar 13C), 80.7 (C_q(CH₃)₃), 66.3–57.4 (NHC_q), 47.3 (CCH₂O), 39.4 (HNCH₂), 36.3 (CH₂(CO)OtBu), 31.1–29.8 (HNC_qCH₂CH₂CONH), 30.9 (HNC_qCH₂), 28.2 (OC(CH₃)₃). MALDI-TOF-MS [M+H₂O]⁺ *m/z* calcd for C₁₇₂H₂₉₇N₁₃O₅₉H₂O: 3509.06, found: 3509.57.

2.2.6. Synthesis of Compound 8

In a Schlenk flask, compound 6 (0.4 mmol, 1.4 g) was dissolved in 30 mL of *N,N*-dimethylformamide, and *N*-methyl-morpholine (1.2 eq, 0.5 mmol, 41.8 mg, 46 μL) was added. The mixture was stirred for 4 h. The excess of *N,N*-dimethylformamide was removed by rotary evaporation, followed by washing with deionized water (10 × 20 mL). The product was further purified by column chromatography using silica gel and dichloromethane:methanol (solvent mixture gradient from 100:0 to 94:6) as eluent. The compound 8 was obtained as a yellow oil in quantitative yield (1.2 g). ¹H NMR (CDCl₃, 600 MHz), δ (ppm): 7.44 (s, CONH, 9H), 5.371 (s, CONH, 9H), 3.93 (s, NH₂), 3.57 (br t, OCH₂CH₂O, 36H), 3.51 (br t, HNCH₂CH₂O, 36H), 3.36 (br t, OCH₂CH₂NH, 18H), 3.26 (br

t, OCH₂CH₂NH, 18H), 2.44 (br t, CH₂(CO)NH, 6H), 2.18 (br t, CH₂(CO)NH, 18H), 1.96 (br t, NHCH₂CH₂(CO)NH, 18H), 1.40 (s, (CO)OC(CH₃)₃, 81H). ¹³C NMR (CDCl₃, 600 MHz), δ (ppm): 173.9 (CH₂(CO)NH), 173.4 (CH₂(CO)NH), 156.3 (NH(CO)OtBu), 79.3 (OC(CH₃)₃), 70.3 (OCH₂CH₂O), 70.2 (CH₂CH₂O), 64.1 (CH₂O), 43.8 (OOCNHC_q), 40.4 (NHCH₂CH₂O), 39.4 (CH₂NH), 30.7 (CH₂CONH), 29.8 (HNC_qCH₂), 28.5 (OC(CH₃)₃). MALDI-TOF-MS [M+Na]⁺ *m/z* calcd for C₁₃₉H₂₆₀N₂₂O₄₈H: 3006.86, found: 3007.80.

2.2.7. Synthesis of Compound 9

In a Schlenk flask, compound 7 (0.48 mmol, 1.69 g) was dissolved in 30 mL of *N,N*-dimethylformamide, and *N*-methyl-morpholine (1.2 eq, 0.58 mmol, 50.6 mg, 50 μL) was added. The mixture was stirred for 4 h. The excess of *N,N*-dimethylformamide was removed by rotary evaporation, followed by washing with deionized water (10 × 20 mL). The product was further purified by column chromatography using silica gel and dichloromethane: methanol (solvent mixture gradient from 100:0 to 94:6) as eluent. The compound 9 was obtained as a yellow oil in quantitative yield (1.57 g). ¹H NMR (CDCl₃, 600 MHz), δ (ppm): 7.26 (s, CONH, 9H), 3.70 (t, *J* = 6 Hz, OCH₂CH₂, 18H), 3.68 (t, *J* = 7.8 Hz, OCH₂CH₂, 18H), 3.61 (m, OCH₂CH₂OCH₂CH₂O, 72H), 3.52 (br t, CH₂O, 18H), 3.37 (br t, NHCH₂, 18H), 2.50 (t, *J* = 7.8 Hz, CH₂(CO)OtBu, 18H), 2.18 (br t, CH₂CO, 24H), 1.97 (br t, HCCH₂, 24H), 1.68 (br t, H₂NC_qCH₂, 6H), 1.41 (s, (CO)OC(CH₃)₃, 81H). ¹³C NMR (CDCl₃, 600 MHz), δ (ppm): 173.7 (NH(CO)OtBu), 171.1 (CH₂(CO)NH), 80.7 (OC(CH₃)₃), 70.6–66.9 (CH₂OCH₂CH₂OCH₂CH₂OCH₂), 58.1 (NH₂C_q), 39.5 (CH₂NH), 36.4 (CH₂CONH), 30.8 (HNC_qCH₂), 28.54(OC(CH₃)₃). MALDI-TOF-MS [M+Na]⁺ *m/z* calcd for C₁₅₇H₂₈₇N₁₃O₅₇H: 3267.99, found: 3269.47.

2.2.8. Synthesis of Compound 10

In an air-free Schlenk flask, compound 4 (1.4 eq, 0.56 mmol, 156.8 mg), *N,N*-diisopropylethylamine (1.4 eq, 0.56 mmol, 72.4 mg, 0.094 mL), and HATU (1.4 eq, 0.56 mmol, 212.9 mg) were dissolved in 20 mL of anhydrous *N,N*-dimethylformamide. The mixture was stirred for 15 min, and compound 8 (0.4 mmol, 1.2 g) was added. The mixture was stirred for 24 h at room temperature under nitrogen atmosphere. The solvent was removed by rotary evaporation and by washing with deionized water (10 × 20 mL). The product was further purified by column chromatography using silica gel and dichloromethane: methanol (solvent mixture gradient from 100:0 to 90:10) as eluent. Compound 10 was obtained as a yellow oil in 95% of yield (1.24 g). ¹H NMR (CDCl₃, 600 MHz), δ (ppm): 7.57 (s, CONH, 9H), 3.60 (br t, OCH₂CH₂O, 36H), 3.51 (br t, HNCH₂CH₂O, 18H), 3.39 (br t, OCH₂CH₂NH, 18H), 3.30 (br t, SCH₂CH₂, 2H), 2.54–2.41 (br t, OCH₂CH₂OCH₂CH₂OCH₂, 10H), 2.33–2.18 CH₂(CO)NH, 2.33 (S(CO)CH₃, 3H), 2.27 (br t, CH₂(CO)NH, 24H), 2.18 (br t, CH₂(CO)NH, 18H), 1.42 (s, (CO)OC(CH₃)₃, 81H). ¹³C NMR (CDCl₃, 600 MHz), δ (ppm): 195.3 (CH₃(CO)S), 173.9 (CH₂(CO)NH), 156.3 (NH(CO)OtBu), 77.3 (OC(CH₃)₃), 70.3 (OCH₂CH₂O), 70.2 (CH₂OCH₂CH₂OCH₂CH₂OCH₂), 64.1 (CH₂O), 40.3 (OOCNHC_q), 39.4 (NHCH₂CH₂O), 39.4 (CH₂NH), 30.7 (CH₂CONH), 29.8 (HNC_qCH₂), 28.5 (OC(CH₃)₃). MALDI-TOF-MS [M+Na]⁺ *m/z* calcd for C₁₅₀H₂₇₈N₂₂O₅₃Na: 3291.9, found: 3291.6.

2.2.9. Synthesis of Compound 11

In an air-free Schlenk flask, compound 4 (1.4 eq, 0.67 mmol, 156.8 mg), *N,N*-diisopropylethylamine (1.4 eq, 0.67 mmol, 86.9 mg, 0.117 mL), and HATU (1.4 eq, 0.67 mmol, 254.7 mg) were dissolved in 20 mL of anhydrous *N,N*-dimethylformamide. The mixture was stirred for 15 min, and compound 9 (0.48 mmol, 1.57 g) was added. The mixture was stirred for 24 h at room temperature under nitrogen atmosphere. The solvent was removed by rotary evaporation and washed with deionized water (10 × 20 mL). The product was further purified by column chromatography using silica gel and dichloromethane: methanol (solvent mixture gradient from 100:0 to 90:10) as eluent. Compound 11 was obtained as a yellow oil in 87% of yield (1.47 g). ¹H NMR (CDCl₃, 600 MHz), δ (ppm): 7.26 (s, CONH, 9H), 3.68 (br t, OCH₂CH₂, 18H), 3.69–3.61 (m, OCH₂CH₂OCH₂CH₂O, 72H), 3.68 (t, *J* = 7.8 Hz,

OCH₂CH₂, 18H), 3.52 (br t, CH₂O, 18H), 3.37 (br t, NHCH₂, 18H), 2.50 (t, *J* = 7.8 Hz, CH₂(CO)OtBu, 18H), 2.28 (br t, CH₂(CO)NH, 2H), 2.31 (s, H₃C(CO)S, 3H), 2.16 (br t, CH₂CO, 24H), 1.97 (br t, HNCH₂, 24H), 1.95 (br t, NHCH₂, 6H), 1.41 (s, (CO)OC(CH₃)₃, 81H). ¹³C NMR (CDCl₃, 600 MHz), δ (ppm): 195.9 (H₃C(CO)S), 173.8 ((CO)OtBu), 171.1 (CH₂(CO)NH), 80.7 (OC(CH₃)₃), 70.6–66.9 (CH₂OCH₂CH₂OCH₂CH₂OCH₂), 58.1 (NH₂C_q), 39.5 (CH₂NH), 36.4 (CH₂CONH), 30.8 (HNC_qCH₂), 28.5 (OC(CH₃)₃).

2.2.10. Synthesis of Compound 12

In a round-bottom flask, compound **10** (0.38 mmol, 1.24 g) was dissolved in 20 mL of deionized water and 80 mL of formic acid. The reaction mixture was stirred for 48 h. The aqueous solution was removed using rotary evaporation. The solid product was solubilized in dichloromethane and washed ten times with a cold saturated sodium carbonate solution. The organic solution was dried with Na₂SO₄, filtered, and the dichloromethane was evaporated yielding the compound **12** as a yellow oil. ¹H NMR (D₂O, 600 MHz), δ (ppm): 9.63, 8.25, and 7.98 (br s, NH, and SH), 3.49 (br s, OCH₂CH₂), 3.25 (br s, NHCH₂), 3.08 (br s, CH₂(CO)NH), 2.08 (br t, CH₂CO), 1.82 (br t, HNCH₂). ¹³C NMR (D₂O, 600 MHz), δ (ppm): 175.8 (CH₂(CO)NH), 69.5–66.4 (CH₂OCH₂CH₂OCH₂CH₂OCH₂), 57.9 (NH₂C_q), 39.0–38.0 (CH₂NH), 37.8 (CH₂CONH), 30.5 (HNC_qCH₂). MALDI-TOF-MS [M+H]⁺ *m/z* calcd for C₁₀₃H₂₀₅N₂₂O₃₄S: 2326.40, found: 2428.02.

2.2.11. Synthesis of Compound 13

In a round bottom flask, compound **11** (0.38 mmol, 1.47 g) was dissolved in 20 mL of deionized water and 80 mL of formic acid. The reaction mixture was stirred for 48 h. The aqueous solution was removed using rotary evaporation. The solid product was solubilized in dichloromethane and washed ten times with a cold saturated sodium carbonate solution. The organic solution was dried with Na₂SO₄, filtered, and the dichloromethane was evaporated yielding the compound **13** as a yellow oil. ¹H NMR (D₂O, 600 MHz), δ (ppm): 7.41 (br s, NH, and SH), 3.74–3.55 (br s, OCH₂CH₂), 2.54 (br s, CH₂(CO)NH), 2.22 (br t, CH₂CO), 2.00 (br t, HNCH₂). ¹³C NMR (D₂O, 600 MHz), δ (ppm): 175.8 (CH₂(CO)NH), 69.5–66.4 (CH₂OCH₂CH₂OCH₂CH₂OCH₂), 57.9 (NH₂C_q), 39.1–38.9 (CH₂NH and CH₂CONH) 29.9 (HNC_qCH₂). MALDI-TOF-MS [M+H]⁺ *m/z* calcd for C₁₃₀H₂₃₁N₁₃O₆₁S: 2982.5 found: 2984.1.

2.3. Nuclear Magnetic Resonance (NMR)

One-dimensional NMR spectra of ¹H and ¹³C were obtained on either a Bruker Avance-III HD 250 MHz, Bruker AVANCE 400, Bruker AVANCE 500, or a Bruker Avance-III 600 MHz spectrometer. The spectra were obtained at 25 °C, and deuterated solvents were used as the lock. Chemical shifts (δ) are reported in parts per million (ppm) using the deuterated solvent residual peaks as the reference.

2.4. Mass Spectrometry (MS)

High-resolution mass spectra were acquired in a Waters Xevo Q-TOF (ESI-QTOF) mass spectrometer. Samples solution in methanol or acetonitrile were injected into the mass spectrometer. Before each analysis, the spectrometer was externally calibrated with phosphoric acid ranging from 98 to 1300 *m/z*. MALDI-TOF mass spectra were recorded on a Bruker Autoflex III MALDI-TOF MS or on a Bruker Microflex II MALDI-TOF MS. Samples were prepared by the dried droplet method, using the universal MALDI-TOF matrix (1:1 mixture of 2,5-dihydroxybenzoic acid and α -cyano-4-hydroxycinnamic acid). A fresh matrix solution was prepared for each experiment at the concentration of 10 mg/mL in acetonitrile and water (1:1, *v/v*) containing 2% of formic acid.

2.5. General Procedure for Functionalization of Gold Nanoparticles

The citrated-stabilized gold nanoparticles with spherical shape and mean diameter of 60 nm were purchased from Sigma–Aldrich as a solution in citrate buffered medium. Both

dendrons were mixed with the gold nanoparticles in a molar ratio of 5 dendrons per 1 AuNP in deionized water, for 48 h at room temperature and under gentle stirring, in the dark. The dendronized gold nanoparticles were purified by dialysis using benzoylated dialysis tubing with 3 kDa molecular weight cut-off (MWCO) to remove the citrate molecules. Approximately 10 cm of the dialysis membrane was washed with deionized water and subsequently loaded with the samples of gold-dendron conjugates. The bags were closed with dialysis tubing clips and placed inside a beaker containing 1 L of deionized water. The outside water was replaced daily for 72 h. After completing the dialysis process, the samples were lyophilized overnight.

2.6. Dynamic Light Scattering (DLS)

The nanoparticles' hydrodynamic diameter and their polydispersity indices (PDIs) were obtained by dynamic light scattering (DLS). Measurements were carried out at 25 °C on a Zetasizer Nano-ZS ZEN3600 instrument (Malvern Instruments) equipped with a 4 mW He-Ne laser with light wavelength of 632.8 nm, and backscattering angle of 173°, using a disposable DTS 1070 cell. The dendronized gold nanoparticles were redispersed by vortexing in deionized water at a concentration of 1 mg/mL. Each sample was analyzed in triplicate.

2.7. Zeta Potential

The zeta potential results are based on the measurement of the velocity of nanoparticles electrophoretic mobility using the laser Doppler anemometry technique. All samples were diluted in ultrapure water at final concentration of 1 mg/mL and the measurements were performed in triplicate at 25 °C using a Zetasizer Nano ZS (Malvern Instruments, Worcester, UK) in a DTS1070 disposable cuvette.

2.8. Absorption Spectroscopy in the UV-Vis

The plasmon surface resonance of the citrate- and dendron-stabilized AuNPs were assessed using an UV-vis spectrometer (Agilent HP 8453, Santa Clara, CA, USA). The lyophilized samples were redispersed using the vortex agitation for 10 min, without further energy to disperse the particles and the spectra were recorded in a 1 cm cell.

2.9. Scanning Electron Microscopy (SEM)

The surface morphology of both dendronized AuNPs was examined using a Quanta 250 field emission scanning electron microscope (FESEM) (FEI Ltd., Natural Bridge Station, VA, USA) operating at an accelerating voltage of 15 kV. Particle samples were prepared by dropping 10 µL of a nanoparticle dispersion at concentration of 1 mg/mL onto a polished silicon wafer. Samples were allowed to dry overnight in the air. The sputters were not coated with a layer of metallic alloy since AuNPs are good electron conducting materials. Under this condition it is possible to visualize the contrast between the organic (dendrons) and metallic portion (AuNPs).

3. Results

In order to obtain NPs with high antimicrobial potential, here we have combined AuNPs with dendrons since both nanostructures possess intrinsic antimicrobial properties. Moreover, the terminal groups on the dendronized AuNP were designed to be negatively or positively charged, which might enhance the antimicrobial activity of these NPs (Figure 1).

Two dendrons were synthesized bearing terminal charged groups, and one thiol moiety at the focal point was responsible for anchoring the dendrons onto the AuNP surface. The amine- and carboxyl-derivative dendrons were designed with polyamide backbones comprising ethylene glycol branches to afford high biodegradability, biocompatibility, and water solubility. Using the AuNPs as a rigid core, it was expected that the peripheral charged groups would remain symmetrically distributed around the AuNPs, enabling an effective interaction between terminal charged groups and the outer membranes of bacteria.

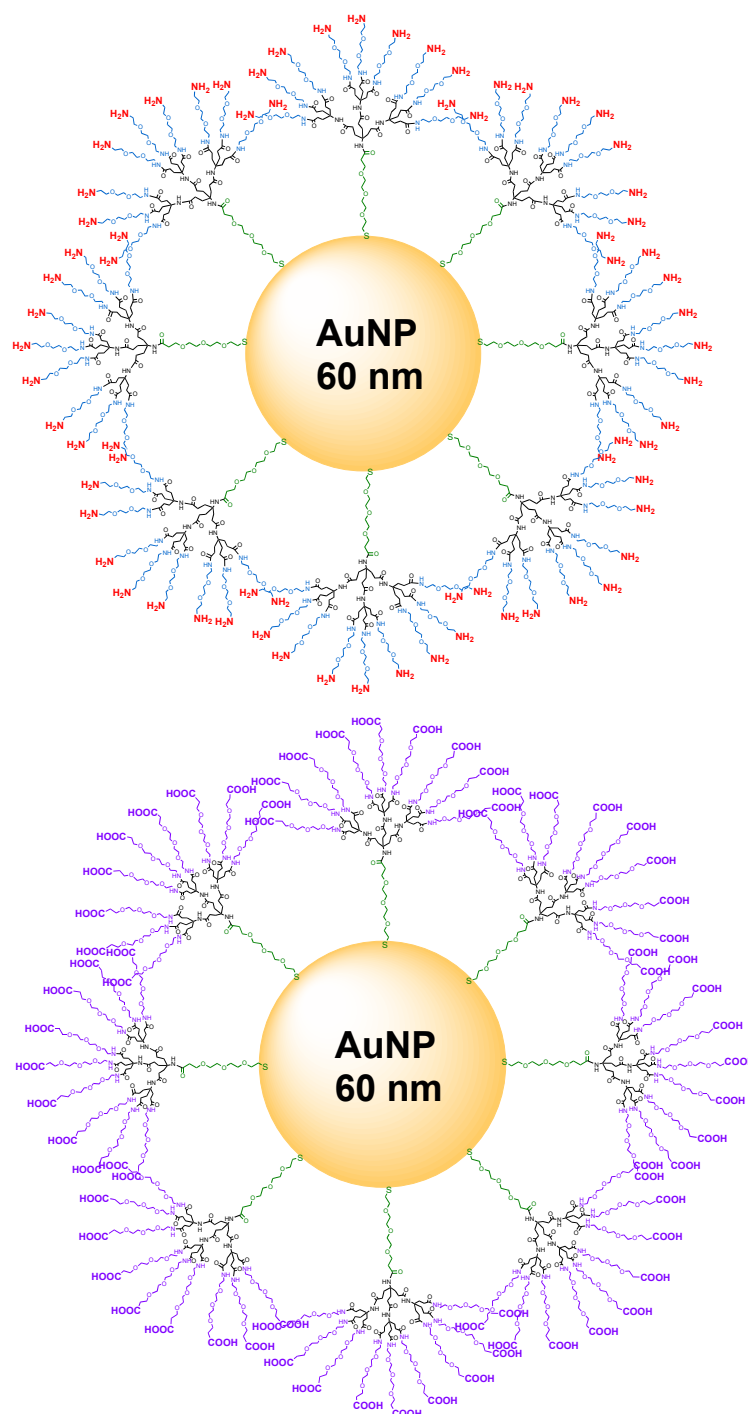
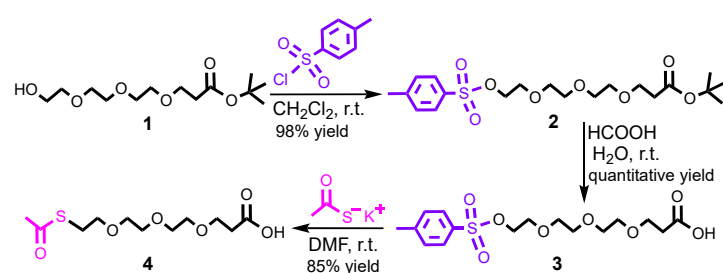


Figure 1. Dendronized gold nanoparticles with amine or carboxylic acid termini synthesized in this work.

Herein, a straightforward synthetic route with a set of efficient reactions was essential to complete the synthesis of the two dendrons. The total synthesis of both dendrons was carried out in seven steps. The spacer **4** bearing a thiol end-group and a carboxylic acid group was synthesized in high global yield. The alcohol group on compound **1** was tosylated to generate compound **2** in 98% yield. The carboxylic acid was deprotected using formic acid, affording compound **3** in quantitative yield. Finally, the tosyl group was substituted with thioacetate to provide the target product **4** in 85% yield (Scheme 1).



Scheme 1. Synthesis of the glycol spacer 4 with a thiol anchoring moiety and a carboxylic acid group.

The ^1H NMR spectrum of compound 4 exhibits a sharp singlet integrating for three protons at 2.33 ppm corresponding to a methyl group adjacent to the carbonyl of thioester. The ^{13}C NMR spectrum of compound 4 shows a signal at 195.9 ppm that is the characteristic shift for thioester carbonyls (see Supplementary Information). The mass spectrum of spacer 4 shows the molecular ion peak $(\text{M}+\text{Na})^+$ at 303.23 m/z (calcd for $\text{C}_{11}\text{H}_{20}\text{O}_6\text{SNa}$: 303.09 m/z) further validating the efficacy of the proposed synthetic route.

The synthesis of the dendrons' backbone was carried out according to a previously published work [52]. Newkome-type backbone with 1 \rightarrow 3 connectivity was built and subsequently functionalized with an amine- or acid carboxylic-glycol derivative (Scheme 2).

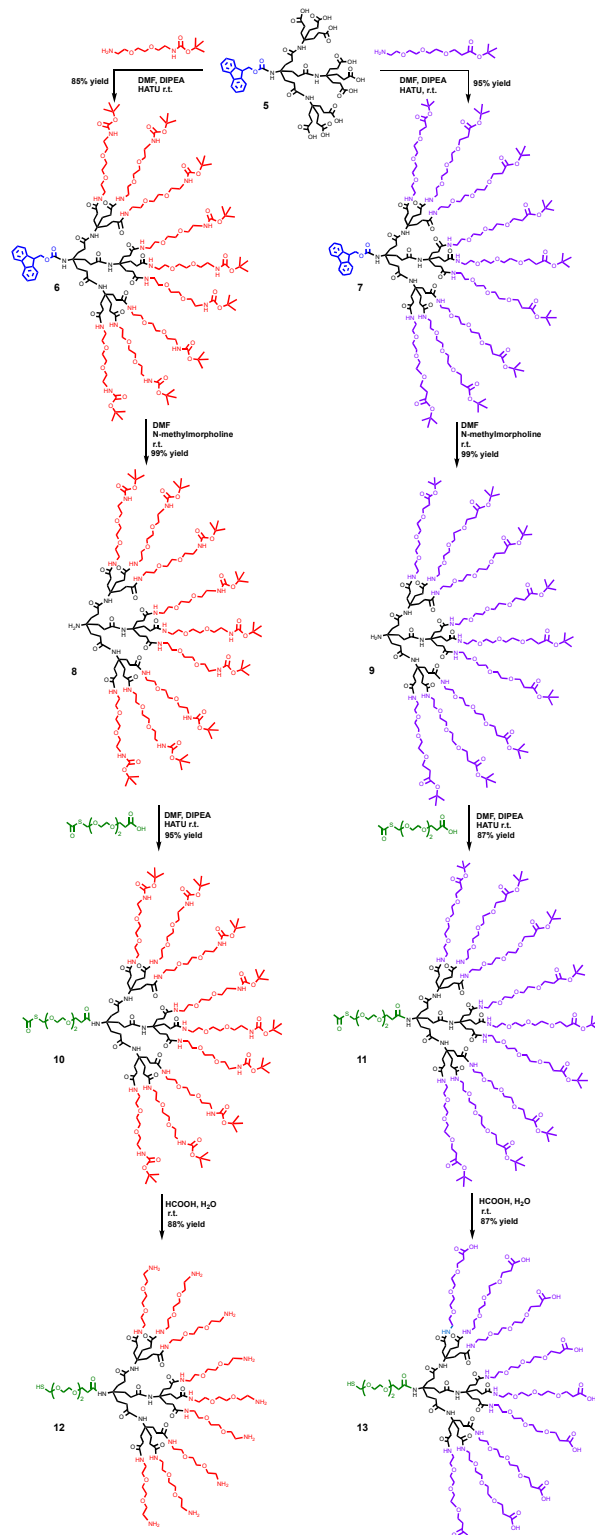
The coupling of *N*-Boc-2,2'-(ethylenedioxy)diethylamine or *tert*-Butyl-12-amino-4,7,10-trioxadodecanoate with dendron five was achieved using HATU, and dimethylformamide (DMF) as solvent in the presence of *N,N*-diisopropylethylamine (DIPEA). The products were purified by column chromatography using dichloromethane:methanol as eluent, yielding compounds 6 and 7 as colorless oils. The Fmoc protecting group was removed using the non-nucleophilic base *N*-methylmorpholine (Scheme 2). The structures of dendrons 6 and 7 were confirmed by NMR spectroscopy and mass spectrometry. In addition to the characteristic peaks of the polyamide scaffold, it is possible to observe signals corresponding to *tert*-butyloxycarbonyl protons. The signals at approximately 3.50 ppm can be attributed to the protons of the ethylene glycol group (see Supplementary Information).

Spacer 4 was coupled to both dendrons using HATU and DIPEA in DMF. The *tert*-butyloxycarbonyl groups of the dendrons' termini were removed using an acidic solution prepared with formic acid. Following the deprotection reaction, the product was dissolved in dichloromethane and washed three times with a saturated sodium carbonate solution. Interestingly, this washing procedure was enough to remove the acetyl group leaving the thiol group unprotected (Scheme 2). Final dendrons 12 and 13 were purified by column chromatography using dichloromethane and methanol, yielding the products as yellowish oils. The target dendrons were characterized by NMR spectroscopy mass spectrometry.

The commercial AuNPs with 60 nm stabilized by citrate were functionalized with the amine- and carboxyl-terminated dendrons through the Au-S bonds. To replace the citrate molecules, both dendrons were stirred in deionized water with the citrate-stabilized AuNPs for 48 h at room temperature, in the dark, in a molar ratio of five dendrons per each AuNP. The AuNPs interact with the amino and carboxyl groups present in the dendron's structures, however considering the higher affinity of the sulfur-gold bond, the functionalization occurs preferably by the thiol group [53–56].

Considering that the exchange of the citrate by dendrons may lead to particle coalescence, the colloidal behavior of the dendronized nanoparticles was assessed by dynamic light scattering (DLS) (Figure 2). The size distribution exhibited a shift to larger diameters upon ligand exchange, indicating partial substitution of the citrate molecules by the dendrons. The hydrodynamic diameter of AuNP–citrate is 60 nm, whereas the hydrodynamic diameter of AuNP–(dendron-NH₂) and AuNP–(dendron-CO₂H) is 109 nm and 80 nm, respectively (Table 1). Indeed, this increase in the hydrodynamic diameter was expected because the dendrons are larger than the citrate molecules. Moreover, due to the ethylene glycol units, the dendronized AuNPs are highly hydrophilic, consequently, the water molecules will strongly interact with the dendrons' branches resulting in a water

layer around the dendronized AuNPs. This solvation phenomenon justifies the increase in the hydrodynamic diameter. Remarkably, despite the presence of free amine or carboxylic acid groups, the size distributions exhibited monomodal profiles with narrow distributions, suggesting that the nanoparticles present low polydispersities and no aggregation.



Scheme 2. Synthesis of two dendrons with a thiol group at the focal point and nine amine or carboxylic acid termini.

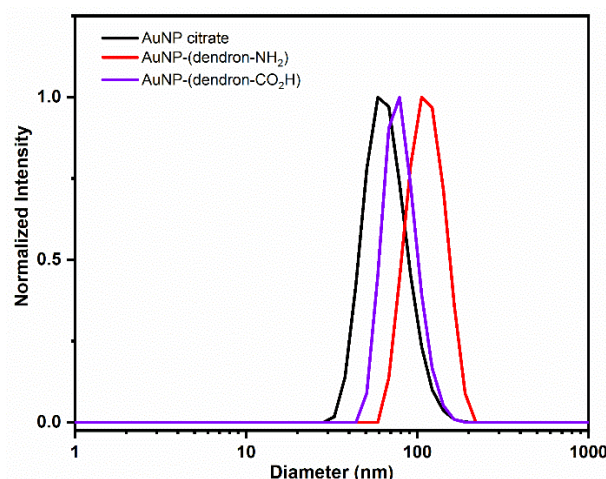


Figure 2. Size distribution profile and the average hydrodynamic diameters obtained by DLS of citrate stabilized AuNPs, cationic dendrimer stabilized AuNPs (AuNP-(dendron-NH₂)), and anionic dendrimer stabilized AuNP (AuNP-(dendron-CO₂H)).

Table 1. Values of zeta potential, hydrodynamic diameter, and PDI obtained by DLS for the AuNPs measured in ultrapure water at 1 mg/mL.

	Zeta Potential (mV ± SD)	Diameter (nm ± SD)	PDI (PDI ± SD)
AuNP-citrate	−49 ± 9	60 ± 2	0.06 ± 0.01
AuNP-(dendron-NH ₂)	27 ± 6	109 ± 1	0.19 ± 0.09
AuNP-(dendron-CO ₂ H)	−31 ± 8	80 ± 1	0.05 ± 0.01

Zeta potential measurements were employed to investigate the surface charge variations upon conjugation of the dendrons to the AuNPs. Briefly, zeta potential corresponds to the electric potential in the interfacial double layer at the slipping plane. In other words, zeta potential is the potential difference between the bulk environment and the stationary shell that surrounds the particle. Zeta potential can provide insights into the superficial charge density of AuNPs [57–59].

The citrate-stabilized AuNPs presented -49 ± 9.1 mV for zeta potential, and when functionalized with the amine-derived dendron this value increased to $+27 \pm 6$ mV, corroborating the proper substitution of citrate molecules. The positive potential zeta was indeed expected since anchoring the thiol group at the metallic surface exposes the positively charged amine groups around the AuNPs.

The zeta potential analysis also evidenced the replacement of citrate molecules by the acid carboxylic-derivative dendron. The zeta potential value shifted from -49 ± 9 mV to -31 ± 8 mV, which is directly associated with a decrease in the particles' electrophoretic mobility [58,60,61]. Considering the negligible changes in the continuous phase, the reduction in the electrophoretic mobility is ascribed to the increment of the hydrodynamic diameter and consequent decrease in the hydrodynamic mobility. The decrease in electrophoretic mobility occurs because larger particles pose a greater retardation force [61]. Moreover, the replacement of citrate molecules by branched macromolecules increases the friction coefficient that acts contrary to electrophoretic mobility.

The morphology of the dendronized AuNPs was investigated by scanning electron microscopy (SEM), which further confirmed the DLS data. The sputters were not coated with a layer of metallic alloy since AuNPs are good electron conducting materials. Under this condition it was possible to visualize the contrast between the organic and metallic portion, that corresponds to the dendron stabilizers and the AuNPs, respectively (Figure 3). The SEM analysis revealed no signal of aggregation phenomena, showing individual AuNPs with a surrounding layer of organic material (dendrons).

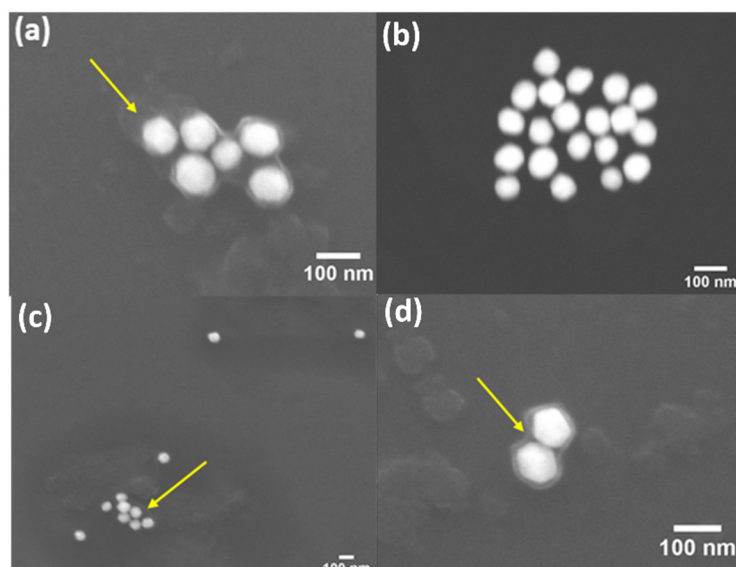


Figure 3. SEM images of AuNPs stabilized by (a,b) cationic dendronized AuNP-(dendron-NH₂), and (c,d) anionic dendronized AuNP-(dendron-CO₂H). The arrows highlight the contrast between the organic stabilizing and the metallic portion.

Developing photothermally active nanomaterials to absorb radiation and generate a local hyperthermic effect is a compelling demand. The plasmonic absorption is not only associated with colloidal stability but also with the photothermal response of metallic nanoparticles. This strategy has been extensively employed for destroying cancer cells, but so far, only to a minimal extent to tackle pathogenic microorganisms. To address this question, we measured the UV-vis absorption of citrate-stabilized and both dendronized AuNPs at the range of 400–800 nm (Figure 4). The UV-vis spectra of citrate- and dendron-stabilized AuNPs reveals the prominent plasmonic band at 560 nm. These intense absorption bands arose from the collective resonant oscillation of the free electrons of the conduction band of the metal [62]. It is important to note that the plasmon band did not shift upon ligand exchange, confirming that the synthesis of the dendronized AuNPs was efficient and did not promote aggregation of the AuNPs.

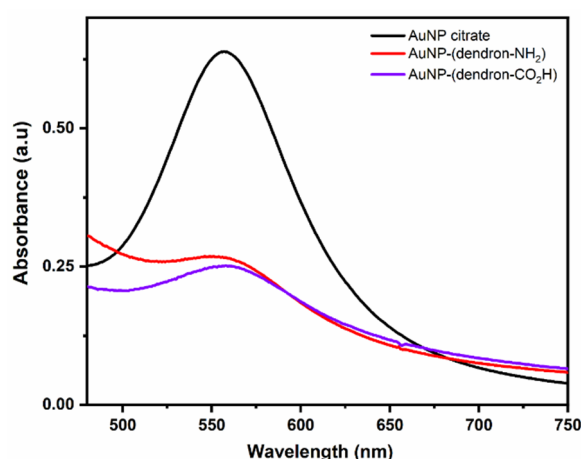


Figure 4. Absorption spectra in the visible region for all AuNPs at 100 μ M in PBS 0.1 M.

4. Conclusions

Two charged polyamide dendrons were designed and synthesized to decorate AuNPs. Amine- and carboxyl-terminated dendrons were both obtained in relatively high yields (38–40%), presenting water solubility, terminal charged groups, and biocompatibility. The functionalization of AuNPs afforded high colloidal stability attested by DLS, SEM, and

UV-vis spectroscopy. Notably, the samples were prepared by only vortexing without further energy to disperse the particles. The DLS technique and SEM showed that the dendronized AuNPs are well dispersed without signal of aggregation or sedimentation. Furthermore, the SEM images revealed a contrast between the organic capping and the metallic portion of the dendronized particles, corroborating the mechanism of nanoparticle functionalization. The synergistic contributions of dendrons with charged termini and AuNPs resulted in promising nanomaterials to tackle antimicrobial resistance. In vitro tests on the antimicrobial activity of these materials against several types of bacteria (Gram-positive and Gram-negative) are currently being carried out.

Supplementary Materials: The following supporting information can be downloaded at: <https://www.mdpi.com/article/10.3390/nano12152610/s1>, Figures S1–S35: NMR and mass spectra for all compounds.

Author Contributions: Conceptualization, G.P., D.L.B. and C.O.; methodology, G.P., D.L.B., D.E.P.S., M.D.R., C.B.B., S.B.A. and C.O.; investigation, G.P., D.L.B., D.E.P.S., M.D.R., C.B.B., S.B.A. and C.O.; writing—original draft preparation, G.P., D.L.B. and C.O.; writing—review and editing, G.P. and C.O.; supervision, C.O.; project administration, C.O.; funding acquisition, C.O. All authors have read and agreed to the published version of the manuscript.

Funding: The authors thank the funding agencies: Sao Paulo Research Foundation (FAPESP: grants #2021/00555-9 and #2018/02093-0 for C.O.; PhD scholarship #2015/04929-0 for D.L.B.; fellowship for C.B.B. #2017/06146-8); National Council for Scientific and Technological Development (CNPq, productivity award for C.O. #311008/2021-6). This study was financed in part by the Coordenação de Aperfeiçoamento de Pessoal de Nível Superior–Brasil (CAPES), finance code 001.

Data Availability Statement: Data is contained within the article or Supplementary Material.

Conflicts of Interest: The authors declare no conflict of interest.

References

1. Ventola, C.L. The Antibiotic Resistance Crisis: Part 2: Management Strategies and New Agents. *Pharm. Ther.* **2015**, *40*, 344–352. [[CrossRef](#)]
2. Ventola, C.L. The Antibiotic Resistance Crisis: Part 1: Causes and Threats. *Pharm. Ther.* **2015**, *40*, 277–283.
3. O'Neill, J. *Tackling Drug-Resistant Infections Globally: Final Report and Recommendations*; Government of the United Kingdom: London, UK, 2016; pp. 1–76.
4. Boucher, H.W.; Talbot, G.H.; Bradley, J.S.; Edwards, J.E.; Gilbert, D.; Rice, L.B.; Scheld, M.; Spellberg, B.; Bartlett, J. Bad Bugs, No Drugs: No ESKAPE! an Update from the Infectious Diseases Society of America. *Clin. Infect. Dis.* **2009**, *48*, 1–12. [[CrossRef](#)]
5. Aminov, R.I. A Brief History of the Antibiotic Era: Lessons Learned and Challenges for the Future. *Front. Microbiol.* **2010**, *1*, 134. [[CrossRef](#)]
6. Eichberg, M.J. Public Funding of Clinical-Stage Antibiotic Development in the United States and European Union. *Health Secur.* **2015**, *13*, 156–165. [[CrossRef](#)]
7. Choi, O.; Deng, K.K.; Kim, N.-J.; Ross, L.; Surampalli, R.Y.; Hu, Z.; Ross, L., Jr.; Surampalli, R.Y.; Hu, Z. The inhibitory effects of silver nanoparticles, silver ions, and silver chloride colloids on microbial growth. *Water Res.* **2008**, *42*, 3066–3074. [[CrossRef](#)] [[PubMed](#)]
8. Cui, Y.; Zhao, Y.; Tian, Y.; Zhang, W.; Lü, X.; Jiang, X. The molecular mechanism of action of bactericidal gold nanoparticles on *Escherichia coli*. *Biomaterials* **2012**, *33*, 2327–2333. [[CrossRef](#)] [[PubMed](#)]
9. Shamaila, S.; Zafar, N.; Riaz, S.; Sharif, R.; Nazir, J.; Naseem, S. Gold Nanoparticles: An Efficient Antimicrobial Agent against Enteric Bacterial Human Pathogen. *Nanomaterials* **2016**, *6*, 71. [[CrossRef](#)]
10. Gupta, A.; Mumtaz, S.; Li, C.-h.H.; Hussain, I.; Rotello, V.M. Combatting Antibiotic-Resistant Bacteria Using Nanomaterials. *Chem. Soc. Rev.* **2019**, *48*, 415–427. [[CrossRef](#)]
11. Rozhin, A.; Batasheva, S.; Kruychkova, M.; Cherednichenko, Y.; Rozhina, E.; Fakhrullin, R. Biogenic Silver Nanoparticles: Synthesis and Application as Antibacterial and Antifungal Agents. *Micromachines* **2021**, *12*, 1480.
12. Garg, P.; Attri, P.; Sharma, R.; Chauhan, M.; Chaudhary, G.R. Advances and Perspective on Antimicrobial Nanomaterials for Biomedical Applications. *Front. Nanotechnol.* **2022**, *4*, 147–159. [[CrossRef](#)]
13. Gao, W.; Zhang, L. Nanomaterials arising amid antibiotic resistance. *Nat. Rev. Microbiol.* **2021**, *19*, 5–6. [[CrossRef](#)] [[PubMed](#)]
14. Pandey, P.; Sahoo, R.; Singh, K.; Pati, S.; Mathew, J.; Pandey, A.C.; Kant, R.; Han, I.; Choi, E.-H.; Dwivedi, G.R.; et al. Drug Resistance Reversal Potential of Nanoparticles/Nanocomposites via Antibiotic's Potentiation in Multi Drug Resistant *P. aeruginosa*. *Nanomaterials* **2022**, *12*, 117. [[CrossRef](#)]

15. Li, X.; Robinson, S.M.; Gupta, A.; Saha, K.; Jiang, Z.; Moyano, D.F.; Sahar, A.; Riley, M.A.; Rotello, V.M. Functional Gold Nanoparticles as Potent Antimicrobial Agents against Multi-Drug-Resistant Bacteria. *ACS Nano* **2014**, *8*, 10682–10686. [[CrossRef](#)] [[PubMed](#)]
16. Shah, M. Gold nanoparticles: Various methods of synthesis and antibacterial applications. *Front. Biosci.* **2014**, *19*, 1320–1336. [[CrossRef](#)] [[PubMed](#)]
17. Okkeh, M.; Bloise, N.; Restivo, E.; De Vita, L.; Pallavicini, P.; Visai, L. Gold Nanoparticles: Can They Be the Next Magic Bullet for Multidrug-Resistant Bacteria? *Nanomaterials* **2021**, *11*, 312. [[CrossRef](#)]
18. Gu, X.; Xu, Z.; Gu, L.; Xu, H.; Han, F.; Chen, B.; Pan, X. Preparation and antibacterial properties of gold nanoparticles: A review. *Environ. Chem. Lett.* **2021**, *19*, 167–187. [[CrossRef](#)]
19. Lee, J.W.; Choi, S.-R.; Heo, J.H. Simultaneous Stabilization and Functionalization of Gold Nanoparticles via Biomolecule Conjugation: Progress and Perspectives. *ACS Appl. Mater. Interfaces* **2021**, *13*, 42311–42328. [[CrossRef](#)]
20. Boisselier, E.; Astruc, D. Gold nanoparticles in nanomedicine: Preparations, imaging, diagnostics, therapies and toxicity. *Chem. Soc. Rev.* **2009**, *38*, 1759–1782. [[CrossRef](#)]
21. Al-Bakri, A.G.; Mahmoud, N.N. Photothermal-Induced Antibacterial Activity of Gold Nanorods Loaded into Polymeric Hydrogel against *Pseudomonas aeruginosa* Biofilm. *Molecules* **2019**, *24*, 2661. [[CrossRef](#)]
22. Peng, L.-H.; Huang, Y.-F.; Zhang, C.-Z.; Niu, J.; Chen, Y.; Chu, Y.; Jiang, Z.-H.; Gao, J.-Q.; Mao, Z.-W. Integration of antimicrobial peptides with gold nanoparticles as unique non-viral vectors for gene delivery to mesenchymal stem cells with antibacterial activity. *Biomaterials* **2016**, *103*, 137–149. [[CrossRef](#)] [[PubMed](#)]
23. Bagga, P.; Siddiqui, H.H.; Akhtar, J.; Mahmood, T.; Zahera, M.; Khan, M.S. Gold Nanoparticles Conjugated Levofloxacin: For Improved Antibacterial Activity over Levofloxacin Alone. *Curr. Drug Deliv.* **2017**, *14*, 1114–1119. [[CrossRef](#)]
24. Payne, J.N.; Waghwan, H.K.; Connor, M.G.; Hamilton, W.; Tockstein, S.; Moolani, H.; Chavda, F.; Badwaik, V.; Lawrenz, M.B.; Dakshinamurthy, R. Novel Synthesis of Kanamycin Conjugated Gold Nanoparticles with Potent Antibacterial Activity. *Front. Microbiol.* **2016**, *7*, 607. [[CrossRef](#)]
25. Daduang, J.; Klaynongsruang, S.; Leelayuwat, C.; Limpaboon, T.; Lulitanond, A.; Boonsiri, P.; Srichan, S.; Soontaranon, S.; Rugmai, S.; Rattanata, N. Gallic acid conjugated with gold nanoparticles: Antibacterial activity and mechanism of action on foodborne pathogens. *Int. J. Nanomed.* **2016**, *11*, 3347–3356. [[CrossRef](#)]
26. Rai, A.; Prabhune, A.; Perry, C.C. Antibiotic mediated synthesis of gold nanoparticles with potent antimicrobial activity and their application in antimicrobial coatings. *J. Mater. Chem.* **2010**, *20*, 6789–6798. [[CrossRef](#)]
27. Dasari, T.P.S.; Zhang, Y.; Yu, H. Antibacterial Activity and Cytotoxicity of Gold (I) and (III) Ions and Gold Nanoparticles. *Biochem. Pharmacol.* **2015**, *4*, 147–161. [[CrossRef](#)] [[PubMed](#)]
28. Zhang, Y.; Shareena Dasari, T.P.; Deng, H.; Yu, H. Antimicrobial Activity of Gold Nanoparticles and Ionic Gold. *J. Environ. Sci. Health Part C* **2015**, *33*, 286–327. [[CrossRef](#)]
29. Ortiz-Benítez, E.A.; Velázquez-Guadarrama, N.; Durán Figueroa, N.V.; Quezada, H.; Olivares-Trejo, J.d.J. Antibacterial mechanism of gold nanoparticles on *Streptococcus pneumoniae*. *Metallomics* **2019**, *11*, 1265–1276. [[CrossRef](#)]
30. Piktel, E.; Suprewicz, Ł.; Depciuch, J.; Chmielewska, S.; Skłodowski, K.; Daniluk, T.; Król, G.; Kołat-Brodecka, P.; Bijak, P.; Pajor-Świerzy, A.; et al. Varied-shaped gold nanoparticles with nanogram killing efficiency as potential antimicrobial surface coatings for the medical devices. *Sci. Rep.* **2021**, *11*, 12546. [[CrossRef](#)]
31. Boisselier, E.; Diallo, A.K.; Salmon, L.; Ornelas, C.; Ruiz, J.; Astruc, D. Encapsulation and Stabilization of Gold Nanoparticles with Click Polyethyleneglycol Dendrimers. *J. Am. Chem. Soc.* **2010**, *132*, 2729–2742. [[CrossRef](#)]
32. Cho, T.J.; Zangmeister, R.A.; MacCuspie, R.I.; Patri, A.K.; Hackley, V.A. Newkome-Type Dendron-Stabilized Gold Nanoparticles: Synthesis, Reactivity, and Stability. *Chem. Mater.* **2011**, *23*, 2665–2676. [[CrossRef](#)]
33. Brunetti, V.; Bouchet, L.M.; Strumia, M.C. Nanoparticle-cored dendrimers: Functional hybrid nanocomposites as a new platform for drug delivery systems. *Nanoscale* **2015**, *7*, 3808–3816. [[CrossRef](#)] [[PubMed](#)]
34. Tomalia, D.A.; Naylor, A.M.; Goddard, W.A. Starburst Dendrimers: Molecular-Level Control of Size, Shape, Surface Chemistry, Topology, and Flexibility from Atoms to Macroscopic Matter. *Angew. Chem. Int. Ed. Engl.* **1990**, *29*, 138–175. [[CrossRef](#)]
35. Astruc, D.; Boisselier, E.; Ornelas, C. Dendrimers Designed for Functions: From Physical, Photophysical, and Supramolecular Properties to Applications in Sensing, Catalysis, Molecular Electronics, Photonics, and Nanomedicine. *Chem. Rev.* **2010**, *110*, 1857–1959. [[CrossRef](#)]
36. Newkome, G.R.; Shreiner, C. Dendrimers derived from 1→3 branching motifs. *Chem. Rev.* **2010**, *110*, 6338–6442. [[CrossRef](#)] [[PubMed](#)]
37. Tomalia, D.A.; Christensen, J.B.; Boas, U. *Dendrimers, Dendrons, and Dendritic Polymers*; Cambridge University Press: Cambridge, UK, 2012; pp. 250–300.
38. Walter, M.V.; Malkoch, M. Simplifying the synthesis of dendrimers: Accelerated approaches. *Chem. Soc. Rev.* **2012**, *41*, 45–93. [[CrossRef](#)] [[PubMed](#)]
39. Ageitos, J.M.; Chuah, J.-A.; Numata, K. Chapter 1. Design Considerations for Properties of Nanocarriers on Disposition and Efficiency of Drug and Gene Delivery; Royal Society of Chemistry (RSC) Publishing: Cambridge, UK, 2016; pp. 1–22.
40. Daniel, M.C.; Ruiz, J.; Nlate, S.; Blais, J.C.; Astruc, D. Nanoscopic assemblies between supramolecular redox active metallo-dendrons and gold nanoparticles: Synthesis, characterization, and selective recognition of H₂PO₄⁻, HSO₄⁻, and adenosine-5'-triphosphate (ATP(2-)) anions. *J. Am. Chem. Soc.* **2003**, *125*, 2617–2628. [[CrossRef](#)]

41. Peña-González, C.E.; García-Broncano, P.; Ottaviani, M.F.; Cangiotti, M.; Fattori, A.; Hierro-Oliva, M.; González-Martín, M.L.; Pérez-Serrano, J.; Gómez, R.; Muñoz-Fernández, M.Á.; et al. Dendronized Anionic Gold Nanoparticles: Synthesis, Characterization, and Antiviral Activity. *Chem. A Eur. J.* **2016**, *22*, 2987–2999. [[CrossRef](#)]
42. Ornelas, C. Brief Timelapse on Dendrimer Chemistry: Advances, Limitations, and Expectations. *Macromol. Chem. Phys.* **2016**, *217*, 148–179. [[CrossRef](#)]
43. Bertuzzi, D.L.; Perli, G.; Braga, C.B.; Ornelas, C. Synthesis, characterization, and anticancer activity of folate γ -ferrocenyl conjugates. *New J. Chem.* **2020**, *44*, 4694–4703. [[CrossRef](#)]
44. Meyers, S.R.; Juhn, F.S.; Griset, A.P.; Luman, N.R.; Grinstaff, M.W. Anionic Amphiphilic Dendrimers as Antibacterial Agents. *J. Am. Chem. Soc.* **2008**, *130*, 14444–14445. [[CrossRef](#)]
45. Hong, S.; Leroueil, P.R.; Majoros, I.J.; Orr, B.G.; Baker, J.R.; Banaszak Holl, M.M. The Binding Avidity of a Nanoparticle-Based Multivalent Targeted Drug Delivery Platform. *Chem. Biol.* **2007**, *14*, 107–115. [[CrossRef](#)]
46. Van Dongen, M.A.; Silpe, J.E.; Dougherty, C.A.; Kanduluru, A.K.; Choi, S.K.; Orr, B.G.; Low, P.S.; Banaszak Holl, M.M. Avidity Mechanism of Dendrimer–Folic Acid Conjugates. *Mol. Pharm.* **2014**, *11*, 1696–1706. [[CrossRef](#)]
47. Karthikeyan, R.; Kumar, P.V.; Koushik, O.S. Dendrimeric Biocides—A Tool for Effective Antimicrobial Therapy. *J. Nanomed. Nanotechnol.* **2016**, *7*, 1–19. [[CrossRef](#)]
48. Perli, G.; Wang, Q.; Braga, C.B.; Bertuzzi, D.L.; Fontana, L.A.; Soares, M.C.P.C.P.; Ruiz, J.; Megiatto, J.D.; Astruc, D.; Ornelas, C.; et al. Self-Assembly of a Triazolylferrocenyl Dendrimer in Water Yields Nontraditional Intrinsic Green Fluorescent Vesosomes for Nanotheranostic Applications. *J. Am. Chem. Soc.* **2021**, *143*, 12948–12954. [[CrossRef](#)] [[PubMed](#)]
49. Abdel-Sayed, P.; Kaeppli, A.; Siriwardena, T.; Darbre, T.; Perron, K.; Jafari, P.; Reymond, J.-L.; Pioletti, D.P.; Applegate, L.A. Anti-Microbial Dendrimers against Multidrug-Resistant *P. aeruginosa* Enhance the Angiogenic Effect of Biological Burn-wound Bandages. *Sci. Rep.* **2016**, *6*, 22020. [[CrossRef](#)]
50. Holmes, A.M.; Heylings, J.R.; Wan, K.-W.; Moss, G.P. Antimicrobial efficacy and mechanism of action of poly(amidoamine) (PAMAM) dendrimers against opportunistic pathogens. *Int. J. Antimicrob. Agents* **2019**, *53*, 500–507. [[CrossRef](#)]
51. Staneva, D.; Grabchev, I. Chapter 20—Dendrimer as antimicrobial agents. In *Dendrimer-Based Nanotherapeutics*; Kesharwani, P., Ed.; Academic Press: Cambridge, MA, USA, 2021; pp. 363–384.
52. Kaufman, E.A.; Tarallo, R.; Elacqua, E.; Carberry, T.P.; Weck, M. Synthesis of Well-Defined Bifunctional Newkome-Type Dendrimers. *Macromolecules* **2017**, *50*, 4897–4905. [[CrossRef](#)]
53. Buhr, E.; Senteleben, N.; Klein, T.; Bergmann, D.; Gnieser, D.; Frase, C.G.; Bosse, H. Characterization of nanoparticles by scanning electron microscopy in transmission mode. *Meas. Sci. Technol.* **2009**, *20*, 100–1010. [[CrossRef](#)]
54. Shan, Y.; Luo, T.; Peng, C.; Sheng, R.; Cao, A.; Cao, X.; Shen, M.; Guo, R.; Tomas, H.; Shi, X. Gene delivery using dendrimer-entrapped gold nanoparticles as nonviral vectors. *Biomaterials* **2012**, *33*, 3025–3035. [[CrossRef](#)] [[PubMed](#)]
55. Abadeer, N.S.; Murphy, C.J. Recent Progress in Cancer Thermal Therapy Using Gold Nanoparticles. *J. Phys. Chem. C* **2016**, *120*, 4691–4716. [[CrossRef](#)]
56. Rajchakit, U.; Sarojini, V. Recent Developments in Antimicrobial-Peptide-Conjugated Gold Nanoparticles. *Bioconjugate Chem.* **2017**, *28*, 2673–2686. [[CrossRef](#)]
57. Hunter, R. *Zeta Potential in Colloid Science: Principles and Applications*; Elsevier Ltd.: Amsterdam, The Netherlands, 1981; pp. 93–117.
58. Ohshima, H. *Encyclopedia of Colloid and Interface Science*; Zeta Potential; Springer: Berlin/Heidelberg, Germany, 2013; pp. 148–207.
59. Perli, G.; Pessoa, A.C.S.N.; Balbino, T.A.; de la Torre, L.G. Ionic strength for tailoring the synthesis of monomodal stealth cationic liposomes in microfluidic devices. *Colloids Surf. B Biointerfaces* **2019**, *179*, 233–241. [[CrossRef](#)]
60. Ottewil, R.H.L.; Rowell, R.L. Colloid Science. In *Zeta Potential in Colloid Science*; Elsevier: Amsterdam, The Netherlands, 1981; pp. 95–120. [[CrossRef](#)]
61. Bhattacharjee, S. DLS and zeta potential—What they are and what they are not? *J. Control. Release* **2016**, *235*, 337–351. [[CrossRef](#)] [[PubMed](#)]
62. Jain, P.K.; Huang, X.; El-Sayed, I.H.; El-Sayed, M.A. Noble metals on the nanoscale: Optical and photothermal properties and some applications in imaging, sensing, biology, and medicine. *Acc. Chem. Res.* **2008**, *41*, 1578–1586. [[CrossRef](#)] [[PubMed](#)]